CHROMOSPHERIC AND CORONAL ACTIVITY IN THE 500-MYR-OLD OPEN CLUSTER M37: EVIDENCE FOR CORONAL STRIPPING?

Alejandro Núñez¹, Marcel A. Agüeros¹, Kevin R. Covey², and Mercedes López-Morales³ DRAFT March 1, 2022

ABSTRACT

We present the results of a spectroscopic survey to characterize chromospheric activity, as measured by $H\alpha$ emission, in low-mass members of the 500-Myr-old open cluster M37. Combining our new measurements of $H\alpha$ luminosities ($L_{H\alpha}$) with previously cataloged stellar properties, we identify saturated and unsaturated regimes in the dependence of the $L_{\rm H\alpha}$ -to-bolometric-luminosity ratio, $L_{\rm H\alpha}/L_{\rm bol}$, on the Rossby number R_o . All rotators with R_o smaller than 0.03 ± 0.01 converge to an activity level of $L_{\rm H\alpha}/L_{\rm bol} = (1.27\pm0.02)\times10^{-4}$. This saturation threshold $(R_{o,\rm sat}=0.03\pm0.01)$ is statistically smaller than that found in most studies of the rotation-activity relation. In the unsaturated regime, slower rotators have lower levels of chromospheric activity, with $L_{\rm H\alpha}/L_{\rm bol}(R_o)$ following a power-law of index $\beta = -0.51 \pm 0.02$, slightly shallower than the one found for a combined ≈ 650 -Myr-old sample of Hyades and Praesepe stars. By comparing this unsaturated behavior to that previously found for coronal activity in M37 (as measured via the X-ray luminosity, $L_{\rm X}$), we confirm that chromospheric activity decays at a much slower rate than coronal activity with increasing R_o . While a comparison of $L_{\rm H\alpha}$ and $L_{\rm X}$ for M37 members with measurements of both reveals a nearly 1:1 relation, removing the mass-dependencies by comparing instead $L_{\rm H\alpha}/L_{\rm bol}$ and $L_{\rm X}/L_{\rm bol}$ does not provide clear evidence for such a relation. Finally, we find that $R_{o,\text{sat}}$ is smaller for our chromospheric than for our coronal indicator of activity ($R_{o,\text{sat}} = 0.03 \pm 0.01 \text{ versus } 0.09 \pm 0.01$). We interpret this as possible evidence for coronal stripping.

Subject headings: Galaxy: open clusters and associations: individual (M37) – stars: activity – stars: chromospheres – stars: low-mass

1. INTRODUCTION

In late-type, main-sequence stars, the rotation rate and the strength of the magnetic field decrease over time (Skumanich 1972; Pallavicini et al. 1981). This is thought to result from a feedback loop in which winds carry angular momentum away from the star, braking its rotation and diminishing the shear between the internal radiative and convective zones, which is responsible for generating the magnetic field (Parker 1993). The resulting, weaker magnetic field then produces weaker winds; these continue to spin down the star and further weaken its magnetic field, but at a diminished rate.

This relationship between age, rotation period (P_{rot}) , and magnetic activity has been modeled empirically with data from the homogeneous, co-eval populations of open clusters. Two of the commonly used tracers of stellar activity are X-ray flux, f_X , which in late-type stars originates in the corona (Vaiana et al. 1981), and $H\alpha$ emission, which originates in the chromosphere (Campbell et al. 1983). Due to their linked heating mechanisms, a correlation is expected between X-ray and $H\alpha$ emission in magnetically active stars.

age-rotation-activity well-calibrated (ARAR) would be particularly valuable for low-mass stars. Earth-like planets are most likely to be discovered in the habitable zones of nearby, old, low-mass, field

stars (cf. discovery of a 1.3 M_{\oplus} planet around Proxima Centauri; Anglada-Escudé et al. 2016). Understanding these planets' radiation environments and potential habitability demands a robust ARAR that could be applied to their parent stars. If we knew the dependence of $P_{\rm rot}$, f_X , or $H\alpha$ on age, a measurement of one of these quantities could be used to determine an accurate age for any isolated field star. Currently, however, we invert the process, adopting canonical ages for field stars to constrain the behavior of the ARAR at the oldest ages (e.g., Kiraga & Stepień 2007; Irwin et al. 2011).

Few open clusters have been systematically surveyed for the three quantities P_{rot} , f_X , and $H\alpha$, and moreover there is a scarcity of accessible clusters older than ≈ 150 Myr. The Hyades and Praesepe (both ≈ 650 Myr) serve as the only anchors for our understanding of the dependence of stellar activity on rotation between a few 100 Myr and the age of field stars ($\gtrsim 2$ Gyr). Unfortunately, the H α - $P_{\rm rot}$ and f_X - $P_{\rm rot}$ relations do not agree for stars in these two clusters: compared to the $H\alpha$ -to-bolometric luminosity ratio $(L_{\rm H\alpha}/L_{\rm bol})$, the X-ray-to-bolometric luminosity ratio $(L_{\rm X}/L_{\rm bol})$ depends much more strongly on $P_{\rm rot}$ for slow rotators (Douglas et al. 2014, hereafter D14). The exact relationship between rotation and activity tracers in a single-aged population remains elusive. Furthermore, the same behavior has been observed in mixed-age samples where different tracers of magnetic activity $(f_X, H\alpha, \text{ and CaII})$ are compared (e.g., Rauscher & Marcy 2006; Stelzer et al. 2013). To understand the physical underpinnings of the ARAR we need to be confident that we understand how different age indicators evolve, and why.

¹ Department of Astronomy, Columbia University, 550 West 120th Street, New York, NY 10027, USA

Department of Physics and Astronomy, Western Washington

University, Bellingham WA 98225, USA

³ Harvard-Smithsonian Center for Astrophysics, 60 Garden Street, Cambridge, MA 02183, USA

The \approx 500-Myr-old open cluster M37 (NGC 2099, 1490±120 pc; Hartman et al. 2008a, hereafter H08), has been extensively surveyed for $P_{\rm rot}$ (Messina et al. 2008; Hartman et al. 2009) and for f_X (Núñez et al. 2015, hereafter Paper I). With more than 400 cluster members with $P_{\rm rot}$ and more than 270 with f_X measurements, M37 is the best laboratory for comparing the behavior of H α emission and of f_X and their relation to $P_{\rm rot}$ in a single-aged population, as there is no other cluster older than the Pleiades (\approx 112 Myr, Stauffer et al. 1998) with comparable $P_{\rm rot}$ and X-ray coverage and as rich a membership (cf. analysis of six other clusters in Núñez & Agüeros 2016).

Here we complement our study in Paper I of the relationship between $P_{\rm rot}$ and f_X in M37 with an examination of the relationship between $P_{\rm rot}$ and H α emission, and therefore between these two tracers of magnetic activity at 500 Myr. To measure H α emission, we obtain optical spectra of 298 M37 members with the 6.5-m telescope at the MMT Observatory, Mt. Hopkins, AZ; 125 of our targets show the line in emission.

In Section 2, we describe how we assembled our cluster membership catalog, our spectroscopic data, and the $P_{\rm rot}$ data we collected from the literature. In Section 3, we characterize stars in M37 using available photometry and our spectra. We present our results in Section 4 before concluding in Section 5.

2. Data

2.1. Cluster Members

H08 obtained g'r'i' images with Megacam on the 6.5 m MMT telescope of a $24' \times 24'$ area centered on M37. These authors then converted the instrumental magnitudes to Sloan Digital Sky Survey (SDSS; York et al. 2000) gri magnitudes for $\approx 16,500$ objects with measurements in all three bands.⁵ The typical one-sigma (σ) error is 0.01 mag, and the magnitude coverage is $10 \lesssim r \lesssim 25$ mag.

In Paper I we used this gri photometry and the distance from the cluster core to identify cluster members. Each star was assigned a probability of being a single member $(P_{\rm s})$, a likely binary member $(P_{\rm b})$, or a field star $(P_{\rm f})$, with $P_{\rm s}+P_{\rm b}\equiv P_{\rm mem}$ and $P_{\rm s}+P_{\rm b}+P_{\rm f}=1$ for each star (see section 3.3 and appendix A of Paper I for details).

We identify 1643 stars with $P_{\text{mem}} \geq 0.2$, which we use as the P_{mem} cutoff for cluster membership. This low P_{mem} threshold may result in our catalog being significantly contaminated by field stars. However, we expect this contamination to be minimal when considering stars with P_{rot} and activity measurements, as field stars tend to be much older and, therefore, very slow rotators unlikely to be detected in the X ray or to have H α emission.

With this in mind, we also search for stars with $0.1 \le P_{\rm mem} < 0.2$ that have ${\rm H}\alpha$ emission in our spectra (see Section 2.2). We found 27 such stars. These stars' location in a color-magnitude diagram (CMD) and

TABLE 1 Description of Columns in M37 Cluster Catalog

Col.	Description					
1	Source ID from H08 (>10000) or Messina et al. (2008) (<10000).					
2, 3	Right ascension and declination of object (J2000). Membership probability. P_{mem}					
4 5	Binary flag from Paper I: 0, likely single star; 1, likely binary.					
6-8	qiJ magnitudes.					
9	Stellar mass.					
10	Rossby number R_0 .					
11,12	EqW and standard deviation of the $H\alpha$ line.					
13-16	EqW and standard deviation of the [NII] λ 6584 and [NII] λ 6548 lines.					
17	Empirical ratio χ of the continuum flux near the H α line and the apparent bolometric flux.					
18	$H\alpha$ -to-bolometric luminosity ratio $L_{H\alpha}/L_{\rm bol}$.					
19	Standard deviation of $L_{\rm H\alpha}/L_{\rm bol}$.					
20	X-ray-to-bolometric luminosity ratio $L_{\rm X}/L_{\rm bol}$.					
21	Standard deviation of $L_{\rm X}/L_{\rm bol}$.					

a mass–H α equivalent width (EqW) plot indicates that their properties are consistent with those of cluster members, and we therefore classify these stars as bona fide M37 members and assign them a $P_{\rm mem}=999$.

Member stars with $P_{\rm b} > P_{\rm s}$ are flagged as likely cluster binaries. As described in Paper I, $P_{\rm b}$ is solely based on photometric distance from the main sequence in the (i, g-i) CMD.

Messina et al. (2008) surveyed M37 in the optical with the 1 m telescope at the Mt. Lemmon Optical Astronomy Observatory, AZ. We use these data to determine whether stars without a counterpart in the H08 survey should be included in our M37 catalog. We determine their membership by visually inspecting their location in the (i, g-i) CMD, using their BV photometry transformed into $gi.^6$ Of the stars identified as cluster members using this approach, we include in our analysis five that have $P_{\rm rot}$ and that have either an X-ray counterpart in Paper I or H α in emission in our Hectospec spectra. We also assign them $P_{\rm mem}=999$.

Table 1 describes the 21 columns in our resulting catalog of cluster members, and Table 2 shows some of these columns for the first five stars in the catalog. This table is available online in its entirety.

2.2. Spectroscopy

We obtained spectra of M37 stars with Hectospec (Fabricant et al. 2005) on the MMT 6.5 m telescope. We used five different fiber configurations, set up using the program XFITFIBS, centered near $\alpha = 05^{\rm h}52^{\rm m}18^{\rm s}$, $\delta = +32^{\circ}33'00''9$ (J2000), to observe 356 stars in the field of view of M37.

We used the 600 line grating, which has a central wavelength of 6500 Å and a free spectral range of 5770 Å, covering the H α line with a spectral resolution $R\approx 1000$. Our targets lie in the range 15.1 < r < 22.6 mag. Stars with $r\gtrsim 20$ mag typically were observed for 300–350 min; stars with $17\lesssim r\lesssim 20$, for 100–300 min; and stars with $17\lesssim 17$, for 1000 min. The median signal-to-noise of our spectra at the H α line core (6563 Å) is 44. Table 3 sum-

⁴ Observations reported here were obtained at the MMT Observatory, a joint facility of the University of Arizona and the Smithsonian Institution.

 $^{^5}$ H08 observed the equatorial Sloan field centered at $03^{\rm h}20^{\rm m}00^{\rm s},$ $00^{\circ}00'00''$ (J2000) to constrain air mass, and then parametrized the instrumental-to-SDSS magnitude relation using a list of observed stars matched to stars extracted from the SDSS Data Release 5 (Adelman-McCarthy et al. 2007).

 $^{^6}$ We used the transformations derived by Jester et al. (2005) and in http://www.sdss.org/dr12/algorithms/sdssUBVRITransform.

TABLE 2 M37 Members

Name	α (J2000)	δ (J2000)	P_{mem}	Bin.	g	i	Mass	Ro	EqW H α	χ	$L_{ m Hlpha}/L_{ m bol}$	$L_{ m X}/L_{ m bol}$
(1)	(2)	°) (3)	(4)	flag (5)	$ \begin{array}{c} (\text{mag}) \\ (6) \end{array} $	(mag) (7)	(M_{\odot}) (9)	(10)	(Å) (11)	(17)	(18)	(20)
140028	88.157125	32.538739	0.77	0	17.09	15.97	1.04		2.01			2.21E-05
140036	88.158163	32.570939	0.59	0	17.48	16.23	1.01	0.08	1.25	9.26E - 05		9.18E - 04
150134	88.186100	32.491900	0.36	0	20.40	18.05	0.63	0.05	-1.89	6.64E - 05	1.26E - 04	1.31E - 03
240167	88.031825	32.524308	0.88	0	20.94	18.46	0.61		-0.70	6.59E - 05	4.62E - 05	7.46E - 04
230343	88.023129	32.546933	0.49	1	23.05	19.80	0.39	0.08	-1.25	2.75E - 05	1.19E - 05	

NOTE. — This table is available in its entirety in the electronic edition of the ApJ. Some columns and rows are shown here for guidance regarding its form and content. Table 1 describes all the columns in this table.

Date	C^{a}	Exp.	Nominal	Num. of	
		(s)	$lpha_{ m J2000}$	$\delta_{ m J2000}$	Spectra
2015-02-18	2	3840	05:52:18.91	+32:31:54.16	134
2015-02-19	2	2810	05:52:18.91	+32:31:54.16	132
2015-02-19	3	2400	05:52:18.64	+32:33:05.93	121
2015-02-20	3	3060	05:52:18.64	+32:33:05.93	123
2015-04-18	1	5400	05:52:11.84	+32:32:45.91	105
2015-09-20	5	3600	05:52:17.96	+32:31:37.13	80
2015-11-21	5	8400	05:52:17.96	+32:31:37.13	80
2015 - 11 - 22	4	3600	05:52:22.40	+32:31:49.42	103

^a Configuration number.

marizes our observations, and Figure 1 shows five example spectra, illustrating the varying strength of the $H\alpha$ line seen in our sample.

The data were reduced automatically by the Telescope Data Center using the HSRED v2.0 pipeline. HSRED performs the basic reduction tasks: bias subtraction, flat-fielding, arc calibration, and sky subtraction.⁷

2.3. Rotation Periods

Messina et al. (2008) and Hartman et al. (2009) published independent surveys of stellar rotation in M37, which we consolidated in Paper I (see sections 3.1 and 3.2 of Paper I for details). Briefly: Messina et al. (2008) used both the Scargle-Press and CLEAN periodogram techniques to measure variability for stars in the range 13 < V < 20 mag and reported $P_{\rm rot}$ values for 120 stars.

Hartman et al. (2009) applied the multiharmonic analysis of variance algorithm of Schwarzenberg-Czerny (1996) to light curves for 15 < r < 23 mag stars included in the Hartman et al. (2008b) list of variable stars. For 372 stars, these authors found that $P_{\rm rot}$ differed <10% when they re-calculated it using only one, two, or three terms of the harmonic series fitted to the light curves. For these stars, they chose $P_{\rm rot}$ calculated using two terms and reported them as "clean" $P_{\rm rot}$ values. As we noted in Paper I, non-clean $P_{\rm rot}$ values add unnecessary ambiguity to our analysis. We therefore include non-clean rotators only if they also have a $P_{\rm rot}$ from Messina et al. (2008) and the two $P_{\rm rot}$ measurements do not differ by more than 20%.

We matched rotators from both surveys using a 10'' matching radius. Individual inspections of the matches comparing the gri photometry from H08 with the BV photometry from Messina et al. (2008) then determined

the most likely correct match. The liberal matching and individual inspection was necessary because the astrometry of objects in Messina et al. (2008) displays a widespread non-linear distortion. For stars with $P_{\rm rot}$ measurements in both surveys, we adopted the $P_{\rm rot}$ from Hartman et al. (2009). Our consolidated list of rotators includes 657 stars with at least one $P_{\rm rot}$ measurement, 426 of which have $P_{\rm mem} \geq 0.2$.

3. DERIVING STELLAR PROPERTIES

3.1. Calculating Masses and $L_{\rm bol}$

We estimate masses for M37 members using the massabsolute r magnitude (M_r) relation of Kraus & Hillenbrand (2007), who generated empirical spectral energy distributions for B8-L0 stars that are calibrated using the 650-Myr-old Praesepe cluster with SDSS ugriz and Two Micron All Sky Survey (2MASS, Skrutskie et al. 2006) JHK photometry (see section 4.1.1 of Paper I). To obtain M_r we estimate the total absorption in r (A_r) using the extinction tables of Schlafly & Finkbeiner (2011) assuming $R_V = 3.1$ and adopting a reddening E(B-V) =0.227 and distance 1490 pc.

Similarly, we estimate $L_{\rm bol}$ for M37 members by using the effective temperature- M_r relation of Kraus & Hillenbrand (2007). After obtaining an effective temperature for each star from M_r , we use the corresponding bolometric correction in the Girardi et al. (2004) tables, which we tailor to the SDSS filter system. This allows us to calculate bolometric magnitudes and luminosities, the latter by again using the distance of 1490 pc to the cluster.

3.2. Measuring H α EqWs and Obtaining $L_{\rm H}\alpha/L_{\rm bol}$

To obtain ${\rm H}\alpha$ EqW measurements for our spectra, we use the PHEW tool, ⁹ which automates the EqW calculation using PySpecKit (Ginsburg & Mirocha 2011) and performs Monte Carlo iterations to obtain EqW uncertainties.

We set 6563 Å as the center of the H α line and define the continuum flux for each spectrum as the average flux between 6540-6558 and 6572-6590 Å. This is modified by eye when the line is broad or shifted away from 6563 Å (e.g., because of binarity or in high radial-velocity objects). In cases where we had more than one spectra for the same star, we weighted-mean combine the spectra before performing the EqW measurement. Lastly, we perform 1000 Monte Carlo iterations to calculate 1σ uncertainties on the EqW measurements. In each iteration,

⁷ See http://mmto.org/~rcool/hsred/index.html for a description of HSRED.

⁸ See section 3.2 of Paper I for details.

⁹ See https://zenodo.org/record/47889#.V5hjMlcZZtI.

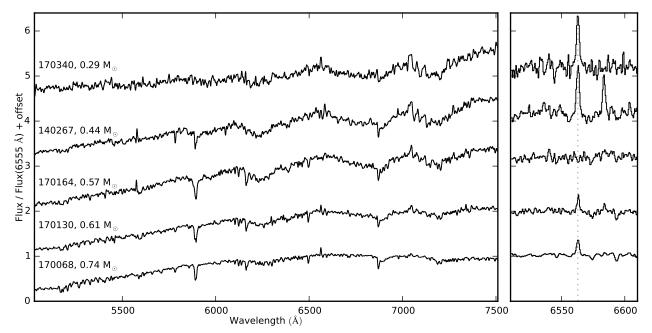


Fig. 1.— Five representative MMT Hectospec spectra of M37 stars, labeled with their H08 designations and photometrically derived masses. Each spectrum is normalized to the flux at 6555 Å and smoothed using a 20 pixel smoothing window. The right panel shows a close-up of the H α line, with the spectra smoothed using a four pixel smoothing window. The vertical dotted line indicates the H α line.

we varied the spectral flux at each pixel by adding a fraction—pulled randomly from a Gaussian distribution—of the intrinsic flux uncertainty. The standard deviation of the 1000 measured EqW values corresponds to the 1σ uncertainties that we report. We measure $H\alpha$ EqW for 294 cluster members; 125 (including 12 likely binaries) show the line in emission.

Figure 2 shows a color-magnitude diagram with stars in the color range 0.2 < (g-i) < 3.7 having $P_{\rm mem} \geq 0.2$. Highlighted in blue (single members) and red (likely binary members) are stars for which we obtain an EqW measurement; negative EqW values correspond to emission. For a handful of stars, our spectra are too noisy to perform a measurement.

D14 studied H α activity for stars in the Hyades and Praesepe. These two benchmark open clusters have similar ages ($\approx 650 \text{ Myr}$) and metallicities, and D14 merged their membership catalogs to create the so-called HyPra cluster. We compare H α activity in M37 and in HyPra in Figure 3. We obtain SDSS r magnitudes for HyPra stars (using a 1" matching radius) to calculate stellar masses using the same Kraus & Hillenbrand (2007) mass- M_r relation we use for M37 stars. Only 20% of HyPra stars in Figure 3 do not have SDSS counterparts; for those we use the stellar masses from D14, which were derived using 2MASS K magnitudes and the Kraus & Hillenbrand (2007) mass-absolute K magnitude relation.¹⁰ We also perform our own EqW measurements for the spectra of these HyPra stars. We exclude from this comparison stars identified as candidate or confirmed binaries.

Figure 3 reveals that $H\alpha$ emission is present in stars with masses up to $\approx 0.8~M_{\odot}$ in M37, whereas in HyPra stars, this limit is $\approx 0.6~M_{\odot}$. The transition from a population of active and inactive stars at a given mass to one where all the stars are active also appears to occur at a

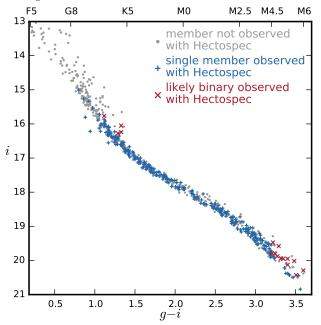


Fig. 2.— CMD for stars in the field of view of M37 with $P_{\rm mem} \geq$ 0.2 in the color range 0.2 < g-i < 3.7. Targets of our MMT Hectospec observations are highlighted in blue (single members) and red (photometrically identified likely binaries).

higher mass in M37 than in HyPra (≈ 0.5 v. ≈ 0.3 M $_{\odot}$). Under the paradigm of chromospheric activity decaying with age, our EqW measurements confirm that M37 is younger than HyPra, as its $\approx 0.6-0.8$ M $_{\odot}$ stars have not yet spun down enough to shut off their chromospheric H α emission.

Strong $H\alpha$ emission can be a sign of flaring. Unfortunately, our Hectospec spectra do not extend sufficiently into the blue to see the rise in the continuum and higher-order Balmer emission lines that are typical of flare spectra (e.g., figure 8 of Agüeros et al. 2009). However, our

 $^{^{10}}$ Our $M_r\text{-}\mathrm{derived}$ masses for HyPra stars are on average 7% smaller than the $M_K\text{-}\mathrm{derived}$ masses given in D14.

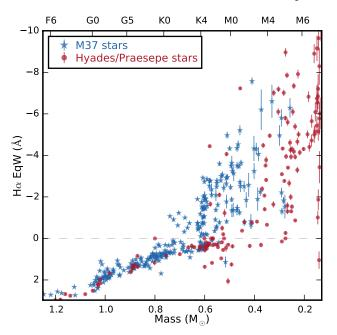


FIG. 3.— ${\rm H}\alpha$ EqW as a function of mass for M37 stars (blue stars symbols) and HyPra stars (red circles). All masses are derived using the absolute magnitude-mass relation of Kraus & Hillenbrand (2007) using SDSS or SDSS-equivalent r magnitudes. All EqW measurements are performed using the PHEW tool. M37 stars identified as likely binaries by Núñez et al. (2015) and HyPra stars identified as candidate or confirmed binaries by D14 and Douglas et al. (2016) are excluded from the plot. ${\rm H}\alpha$ activity is evident in higher-mass stars in M37 than in HyPra, indicating that M37 is indeed the younger cluster.

inspection of the continuum between 5000 and 6000 Å suggests it is unlikely that we caught any of these stars during a significant flare.

For all M37 stars with $H\alpha$ emission, we derive $L_{\rm H\alpha}/L_{\rm bol}$. This quantity is frequently used to compare levels of chromospheric activity between stars in samples spanning a range of masses, as it indicates the significance of $H\alpha$ flux relative to the entire energy output of the star. $L_{\rm H\alpha}/L_{\rm bol}$ can be obtained by using the relation

$$L_{\rm H\alpha}/L_{\rm bol} = -W_{\rm H\alpha} \frac{f_0}{f_{\rm bol}},\tag{1}$$

where $W_{\mathrm{H}_{\alpha}}$ is the $\mathrm{H}\alpha$ EqW, f_0 is the continuum flux near the $\mathrm{H}\alpha$ line, and f_{bol} is the apparent bolometric flux.

For non-flux-calibrated spectra such as our Hectospec spectra, an alternative approach is to calculate $\chi=f_0/f_{\rm bol}$ as a function of color. D14 derived an empirical relation between χ and color using spectra from the Phoenix Aces model spectra (Husser et al. 2013) with solar metallicity, $\log(g)=5.0$, and $2500 \leq T_{\rm eff} \leq 5200$. We use that relation to derive χ values for our M37 stars by linearly interpolating between the D14 colors. For stars with a 2MASS counterpart, we use their dereddened (i-J) colors (requiring that the photometric quality be "C" or better); for stars with no 2MASS counterparts, we use de-reddened (g-i) instead.¹¹

3.3. Accounting for Contamination by an Emission Nebula

Some of the Hectospec spectra exhibit [NII] λ 6548 and λ 6584 Å emission. [NII] emission is known to originate in warm gas clouds, with temperatures near 10⁴ K and atomic hydrogen densities around 10² – 10⁴ cm⁻³.

It is unlikely that the M37 stars are responsible for this emission, as they are not luminous enough to generate Strömgren spheres (Strömgren 1939). A more likely source is a foreground emission nebula, given the apparent extent of the emission near the core of M37 and the strength of the [NII] lines with respect to that of the stellar spectra. Unfortunately, our Hectospec spectra do not have enough wavelength resolution to perform velocity measurements, and we are not able to measure radial velocity differences between the nebula and the M37 stars.

We measured the EqW of the [NII] emission lines using the same technique described in Section 3.2. Figure 4 shows a mosaic of $H\alpha$ images from the Isaac Newton Telescope Photometric $H\alpha$ Survey (IPHAS) of the Northern Galactic Plane (Drew et al. 2005) covering the core of M37. A white cross indicates the center of the cluster. For a sense of scale, we draw a white circle marking a 10' radius from the cluster center. Spectra with [NII] λ 6584 EqW < -3.0 are indicated with red x symbols; spectra with $-3.0 \leq [NII]\lambda$ 6584 EqW ≤ 0.5 , with orange crosses; and spectra with $-0.5 < [NII]\lambda$ 6584 EqW ≤ 0 , with blue circles. Most spectra with strong [NII] emission coincide with the location of a dim nebular structure (northeast of the cluster center). Five examples of our spectra with [NII] emission lines are shown in Figure 5.

Since the ionization potential energy of N is very similar to that of H, H α emission in principle always accompanies [NII] emission in emission nebulae. This means that some of our H α EqW measurements for M37 stars may be contaminated by H α emission from the nebula.

Observations of many different planetary nebulae show that the intensity ratio [NII] $\lambda 6584/H\alpha$ can vary significantly, from 0 to ≈ 4 (see, e.g., White 1952; Kaler 1983), depending on the metal content and density of the nebula (Draine 2011). It is, therefore, difficult to use this ratio alone to characterize the nature of the nebula (Frew & Parker 2010). Furthermore, the $[OIII]\lambda 4959$ and $\lambda 5007$ Å lines that are also typical of emission nebulae, and that are useful in determining gas density and temperature, fall outside the wavelength range of our Hectospec spectra, thus preventing us from characterizing the nebula. We cannot determine the amount of nebular $H\alpha$ emission contaminating our stellar spectra. We therefore exclude cluster stars with strong [NII] emission ([NII] $\lambda 6584$ EqW < -3.0, henceforth referred simply as [NII] contamination) from our analysis.

3.4. Calculating Rossby Numbers

Noyes et al. (1984) found that to study the relation between rotation and activity, using $R_o = P_{\rm rot}/\tau$, where τ is the convective turnover time, rather than $P_{\rm rot}$ directly yields easier-to-interpret results, as it removes the mass dependence observed in stars with saturated levels of activity. In Paper I we estimated τ values for M37 members using the empirical stellar mass- τ relation of Wright et al. (2011), which is based on $P_{\rm rot}$ and $L_{\rm X}$ measurements of

 $^{^{11}}$ We derive giJ extinction values using the tables of Schlafly & Finkbeiner (2011), assuming $R_V=3.1$ and adopting a reddening E(B-V)=0.227 (H08).

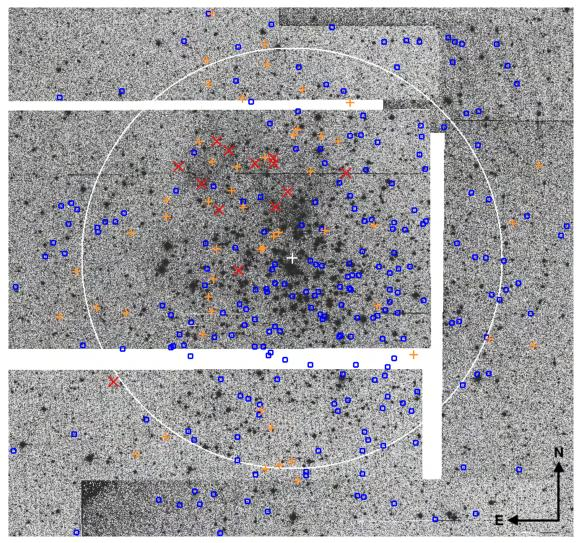


Fig. 4.— Mosaic of IPHAS H α images of M37 spanning 0.52 degrees in RA and 0.42 in DEC. North is up and East is to the left. To provide a sense of scale, the white circle marks the 10' radius from the cluster center (white cross). Red x symbols indicate spectra with [NII] λ 6584 EqW < -3.0, orange crosses, spectra with -3.0 \leq [NII] λ 6584 EqW < -0.5, and blue circles, spectra with -0.5 \leq [NII] λ 6584 EqW \leq 0.

over 800 stars in the mass range $0.09-1.36~{\rm M}_{\odot}.^{12}$ With those τ values we calculated R_o for all M37 members with $P_{\rm rot}$. Here we use these same τ and R_o values to study the rotation-activity relation in H α space.

4. RESULTS AND DISCUSSION

4.1. Relationship Between $H\alpha$ Emission and Rotation

To study the relationship between chromospheric activity and stellar rotation, we perform a similar analysis as in Paper I, where we parametrized the $L_{\rm X}/L_{\rm bol}-R_o$ relation as a flat region connected to a power-law. Here, we fit this same functional form to $L_{\rm H\alpha}/L_{\rm bol}$:

$$\frac{L_{\text{H}\alpha}}{L_{\text{bol}}} = \begin{cases} \left(\frac{L_{\text{H}\alpha}}{L_{\text{bol}}}\right)_{\text{sat}} & \text{if } R_o \le R_{o,\text{sat}} \\ CR_o^{\beta} & \text{if } R_o > R_{o,\text{sat}} \end{cases}$$
(2)

where $(L_{\text{H}\alpha}/L_{\text{bol}})_{\text{sat}}$ is the activity saturation level, $R_{o,\text{sat}}$ is the saturation threshold, β is the power-law in-

dex characterizing the unsaturated regime, and C is a constant. We fit this model to the 65 single cluster members that have both R_o and $L_{\rm H\alpha}/L_{\rm bol}$ measurements and do not have significant [NII] contamination.

We convert the model in Equation 2 into log-space for the fit and assume flat priors over all three parameters. We use the Markov-chain Monte Carlo (MCMC) package $emcee^{13}$ (Foreman-Mackey et al. 2013) to carry out the fit. emcee builds posterior probability distributions for each parameter by performing a random walk in parameter space. This same approach was used in Paper I and by D14 for their sample of HyPra H α emitters. We use 300 initial seeds and 3000 iterations, one tenth of which were to burn-in the walkers.

Shown in gray lines in Figure 6 are 200 models drawn at random from the posterior probability distributions. The solid black line indicates the most probable model, i.e., the maximum a posteriori model. The resulting best-fit parameters are $(L_{\rm H\alpha}/L_{\rm bol})_{\rm sat}=(1.27\pm0.02)\times10^{-4},$ $R_{o,\rm sat}=0.03\pm0.01,$ and $\beta=-0.51\pm0.02.$ The parameters are

 $^{^{12}}$ We chose to use the fitted values of Wright et al. (2011) based on $\beta=-2.0$ instead of -2.7, as we questioned in Paper I the validity of the "unbiased" sample from which these authors obtained $\beta=-2.7.$

¹³ http://dan.iel.fm/emcee/current/

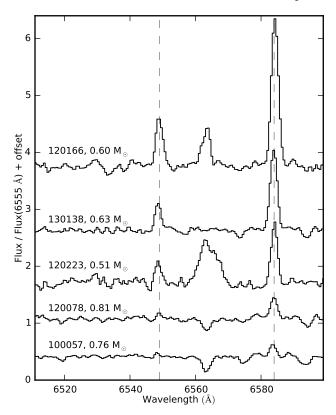


Fig. 5.— Five M37 stars where [Nii] emission is observed, labeled with their H08 designations and photometrically derived masses. Each spectrum is normalized to the flux at 6555 Å and smoothed using a four pixel smoothing window. The dashed vertical lines indicate the [NII] λ 6548 and λ 6584 Å doublet.

ter values correspond to the $50^{\rm th}$ quantile, and the uncertainties correspond to the $16^{\rm th}$ and the $84^{\rm th}$ quantiles (for consistency with 1σ Gaussian uncertainties). We highlight in Figure 6 single cluster members with strong [NII] contamination, but we exclude them from the fit analysis. Figure 7 shows the posterior probability distributions for all parameters.

4.1.1. Sensitivity of Results to Choices of $P_{\rm mem}$ and [NII] Contamination Thresholds

We test how sensitive our MCMC results are to the two parameters used to define our sample of stars, namely, $P_{\rm mem}$ and [NII] contamination. We re-run our fit using a more conservative $P_{\rm mem}=0.7$ cutoff instead of our adopted 0.2, and also adopting a more conservative [NII] $\lambda 6584$ EqW = -1.0 cutoff instead of -3.0. In both cases, the new $R_{o,\rm sat}$ and β values are within 1σ of our original best-fit results, underlining their reliability.

4.1.2. Comparison to Previous Results

The saturation level $(L_{\rm H\alpha}/L_{\rm bol})_{\rm sat} = (1.27\pm0.02) \times 10^{-4}$ for M37 stars is the same, within the errors, as the one found by D14 for HyPra stars, $(1.26\pm0.04) \times 10^{-4}$. The saturated regime includes stars with R_o numbers up to 0.03 ± 0.01 . This saturation threshold is smaller by at least a factor of two than the typical value found in other sets of stars. For example, D14 found $R_{o,\rm sat} = 0.11^{+0.02}_{-0.03}$ using H α activity measurements of HyPra stars, Jackson & Jeffries (2010) found $R_{o,\rm sat} \approx 0.1$ using CaII activity measurements of NGC 2516 stars, and Randich (2000)

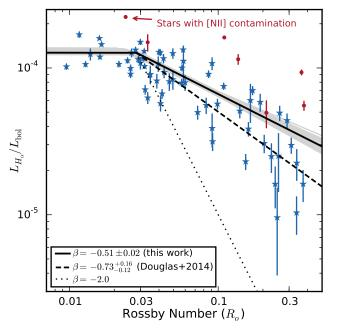


FIG. 6.— $L_{\rm H}\alpha/L_{\rm bol}$ as a function of Rossby number R_o for M37 single cluster members. The solid black line is the maximum a posteriori fit from the MCMC algorithm for the model described by Equation 2. The gray lines are 200 random samples from the posterior probability distributions. The dashed line indicates the fit found by D14 on a sample of HyPra stars. The dotted line indicates a slope of -2.0, which is typically found in studies of X-ray activity indicators. Red circles indicate cluster stars with [NII] contamination ([NII] λ 6584 EqW < -3.0, see Section 3.3); these stars are excluded from our analysis.

found $R_{o,\mathrm{sat}} \approx 0.16$ using X-ray activity measurements of a heterogeneous sample of field and cluster stars. More surprisingly, in Paper I we found that $R_{o,\mathrm{sat}} = 0.09 \pm 0.01$ for our sample of X-ray-emitting M37 stars.

In the unsaturated regime, $\mbox{H}\alpha$ activity decreases as a power-law with slope $\beta=-0.51\pm0.02$. This slope is statistically shallower than the $\beta=-0.73^{+0.16}_{-0.12}$ that D14 found for HyPra stars. In turn, the β values found in these two studies of $\mbox{H}\alpha$ activity are significantly shallower than the values found in studies of X-ray activity. For example, Güdel et al. (1997) found $\beta=-2.64\pm0.12$ for a sample of 12 solar-type stars of ages 0.07 to 9 Gyr, while Randich (2000) and Wright et al. (2011) found $\beta=-2.10\pm0.09$ and -2.18 ± 0.16 , respectively, for X-ray samples of field and cluster stars. And in Paper I we found $\beta=-2.03^{+0.17}_{-0.14}$ in our *Chandra* study of M37.

4.2. Chromospheric versus Coronal Activity

A difference between the decay of H α and X-ray emission has been observed before (e.g., Hodgkin et al. 1995; Preibisch & Feigelson 2005; Stelzer et al. 2013). Our results confirm this discrepancy and highlight a physical distinction between the decay rate of chromospheric activity versus coronal activity in low-mass stars. Furthermore, since $R_{o,\rm sat}$ is smaller for $L_{\rm H}\alpha/L_{\rm bol}$ versus R_o than for $L_{\rm X}/L_{\rm bol}$ versus R_o , our results indicate that as stars spin down, their chromospheres exit the saturated regime before their coronae do. This leads us to examine our H α and X-ray data in more detail.

Figure 8 shows $P_{\rm rot}$ versus stellar mass for M37 stars, including both single (blue star symbols) and likely binary members (red triangles). Stars with detected H α

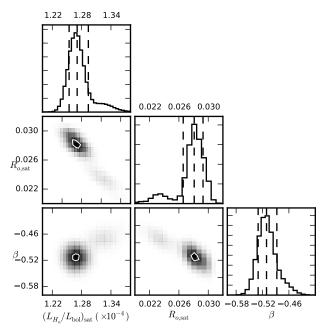


FIG. 7.— Marginalized posterior probability distributions from the MCMC analysis using emcee. The parameter values of the a posteriori model are the peaks of the one-dimensional distributions; the vertical dashed lines approximate the median and 68-percentiles. The two-dimensional distributions illustrate covariances between parameters; the white contour lines approximate the 68-percentile of the distributions.

emission have their symbols filled, and stars with detected X-rays are highlighted with a green circle. In total there are 50 stars with both ${\rm H}\alpha$ and X-ray emission (nine are likely binaries), all with masses $\leq 0.73~{\rm M}_{\odot}$; of these, 24 have $P_{\rm rot}$ measurements.

Most active low-mass stars should have some level of ${\rm H}\alpha$ emission. The fact that we do not detect this emission for stars with masses >0.73 ${\rm M}_\odot$ in our M37 sample may be because ${\rm H}\alpha$ absorption, which increases in intensity with stellar mass (Cram & Mullan 1985), dominates the ${\rm H}\alpha$ spectral feature in those stars. In principle it is possible to separate the levels of ${\rm H}\alpha$ emission and absorption, but our spectra do not have the necessary resolution to perform this exercise. We therefore concentrate on stars for which we measure ${\rm H}\alpha$ emission using the approach described in Section 3.2.

Figure 9 compares the activity of M37 stars—excluding likely binaries and stars with [NII] contamination— in $H\alpha$ and in X rays. We use the 0.1–2.4 keV $L_{\rm X}$ values derived in Paper I. In the left panel, where $L_{\rm H\alpha}$ is plotted versus $L_{\rm X}$, there is a clear positive correlation between the two indicators of activity in our co-eval sample of M37 stars, in spite of the noncontemporaneous nature of the observations. A least squares bisector regression¹⁴ indicates that $L_{\rm X}$ is proportional to $L_{\rm H\alpha}$ following a power-law such that $L_{\rm X} \propto L_{\rm H\alpha}{}^{\alpha}$, where $\alpha = 1.08 \pm 0.02$ (black dashed line). The Pearson correlation coefficient r = 0.80 for this relation suggests that the two quantities are strongly correlated.

Martínez-Arnáiz et al. (2011) found a steeper power-

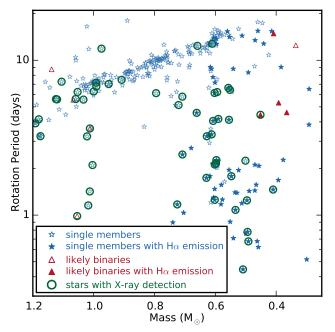


FIG. 8.— $P_{\rm rot}$ versus mass for M37 members. Single stars are indicated with blue symbols, and likely binaries with red triangles. Stars with H α emission have their symbols filled. Stars with X-ray emission identified in Paper I are highlighted with a green circle.

law slope of 1.60 ± 0.07 for a sample of F- to M-type stars. Using only M-dwarfs from that same study, Stelzer et al. (2012) found a power-law slope of 1.29 ± 0.15 . Similarly, Stelzer et al. (2013) found a steeper power-law slope of 1.61 ± 0.23 for a sample of nearby (<10 pc) M dwarfs. Pace & Pasquini (2004), on the other hand, did not find a correlation between $L_{\rm X}$ and chromospheric activity, the latter measured as the flux of H and K lines of CaII (their figure 8, left panel), for a sample of HyPra stars.

In Figure 9 we color-code stars by mass. The left panel shows a clear dependence of $L_{\rm H\alpha}$ and $L_{\rm X}$ on mass. This is not surprising, since surface area increases with mass along the main sequence. In the right panel we divide both luminosities by $L_{\rm bol}$ to remove this mass dependence. Once we do this, the H α -X-ray activity correlation is not as clear: a least squares bisector regression gives $\alpha=1.05\pm0.01$. Its Pearson r=0.63 indicates that the $L_{\rm H\alpha}/L_{\rm bol}-L_{\rm X}/L_{\rm bol}$ correlation is not as strong as with $L_{\rm H\alpha}-L_{\rm X}$. Furthermore, if we exclude the two outliers in this panel (the two 0.5–0.6 M $_{\odot}$ stars well above/below the main locus), α decreases to 0.89 \pm 0.01 and the Pearson r decreases to 0.43.

This apparent stagnation of $L_{\rm X}/L_{\rm bol}$ with respect to changes in $L_{\rm H\alpha}/L_{\rm bol}$ is more evident in Figure 10, in which both panels include only M37 stars with both $L_{\rm H\alpha}$ and $L_{\rm X}$ measurements. The vertical dashed lines indicate the two saturation thresholds: $R_{o,{\rm sat}}=0.03$ for the $L_{\rm H\alpha}/L_{\rm bol}-R_o$ relation, and $R_{o,{\rm sat}}=0.09$ for $L_{\rm X}/L_{\rm bol}-R_o$ (from Paper I). Coronal emission saturates at slower $P_{\rm rot}$ than chromospheric emission.

A larger $R_{o,\mathrm{sat}}$ value for $L_{\mathrm{X}}/L_{\mathrm{bol}}$ can be interpreted as evidence for coronal stripping. This mechanism is sometimes invoked to explain the saturation level observed in $L_{\mathrm{X}}/L_{\mathrm{bol}}$, in which centrifugal forces strip the outermost layers of the corona (e.g., Christian et al. 2011; Argiroffi et al. 2016). It is possible that coronal stripping is also partially driven by an imbalance between magnetic and

¹⁴ The least squares bisector regression treats both the dependent and independent variables symmetrically. Therefore, it is the most appropriate method to use in this case, since we are interested in the underlying theoretical relationship between the two quantities (see Isobe et al. 1990).

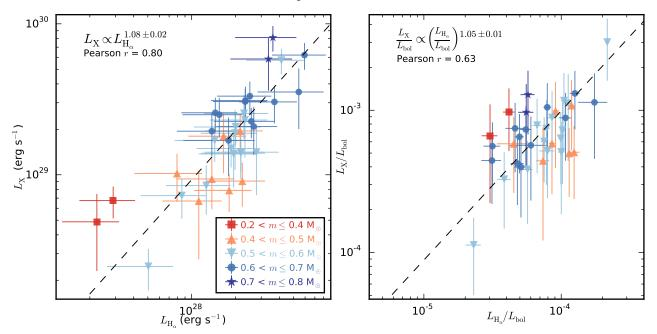


FIG. 9.— Left: L_X versus $L_{\text{H}\alpha}$ for single members of M37. Right: $L_{\text{H}\alpha}$ as a fraction of L_{bol} versus L_X as a fraction of L_{bol} for the same stars. In both panels, red stars have masses between 0.2 and 0.4 M_{\odot} , orange stars between 0.4 and 0.5, light blue stars between 0.5 and 0.6, blue stars between 0.6 and 0.7, and dark blue stars between 0.7 and 0.8. In both panels, the power-law relation and the Pearson r found with a least squares bisector regression is annotated on top and indicated with a black dashed line.

plasma pressure equilibrium, in a scenario with highly energetic stellar winds (e.g., Parker 1960; Jardine & Unruh 1999).

The potential coronal stripping seen in M37 stars may point to the fact that coronal indicators such as X rays present limitations as tracers of stellar activity. Tracers that originate closer to the stellar surface (e.g., measurements of photospheric or chromospheric emission) are perhaps more representative of the magnetic heating mechanism in the stellar atmosphere. Indeed, Davenport (2016) found a similar $R_{o,\text{sat}} \approx 0.03$ in a study of stellar flares measured from Kepler light curves of \approx 290 stars. Furthermore, studies including other chromospheric tracers (e.g., CaII or MgII emission) find no evidence for supersaturation (e.g., Christian et al. 2011), supporting the idea that stripping mechanisms do not affect the inner atmospheric layers.

It would be valuable to study other indicators of chromospheric activity for the same sample of M37 stars. The correlation between H α emission and other chromospheric indicators has been found to be ambiguous at best (e.g., Strassmeier et al. 1990; Scandariato et al. 2016). However, if $R_{o,\text{sat}}$ for other chromospheric indicators agreed with the one we find for H α , it would highlight the limitation of X rays as a reliable estimator of stellar activity. Chromospheric indicators may have more predictive power in the parametrization of the rotationactivity relation and, ultimately, the ARAR.

5. SUMMARY

We present the results of a spectroscopic survey to characterize chromospheric activity, as measured by $H\alpha$ emission, in low-mass members of the 500-Myr-old open cluster M37. We measured $H\alpha$ EqWs for 294 cluster members, 125 of which show the line in emission.

We use properties previously cataloged for M37's members in Paper I, including P_{mem} , mass, $L_{\rm bol}$, and τ , and

 P_{rot} measurements from Messina et al. (2008) and Hartman et al. (2009) to examine the dependence of activity on rotation in this cluster.

An emission nebula appears to have contaminated a small fraction of our spectra, namely in the form of strong [NII] $\lambda 6548$ and $\lambda 6584$ Å emission lines, and potentially some H α emission as well. We exclude from our rotation-activity analysis cluster stars for which this contamination is strong.

M37 stars exhibit $H\alpha$ emission in stars as massive as $\approx 0.8~M_{\odot}$, compared to $\approx 0.6~M_{\odot}$ in the ≈ 650 -Myr-old merged Hyades/Praesepe sample of stars (Douglas et al. 2014). This confirms that M37 is younger than these two clusters.

We identify saturated and unsaturated regimes in the dependence of $L_{\rm H\alpha}/L_{\rm bol}$ on R_o . Rotators with R_o less than the saturation threshold $R_{o,\rm sat}=0.03\pm0.01$ are saturated, and converge to an activity level of $L_{\rm H\alpha}/L_{\rm bol}=(1.27\pm0.02)\times10^{-4}$. This $R_{o,\rm sat}$ is statistically smaller than the canonical $R_o=0.1$ found in most studies of the rotation-activity relation. Only the study of flaring M dwarfs by Davenport (2016) finds a comparably small $R_{o,\rm sat}$.

In the unsaturated regime, faster rotators have increasing levels of chromospheric activity, with $L_{\rm H\alpha}/L_{\rm bol}(R_o)$ following a power-law of index $\beta=-0.51\pm0.02$, slightly shallower than the one found by Douglas et al. (2014) for Hyades/Praesepe stars. We confirm previous findings that show chromospheric activity decaying at a much slower rate than coronal activity with increasing R_o .

While a comparison of $L_{\rm H\alpha}$ and $L_{\rm X}$ for M37 stars with measurements of both reveals a close to 1:1 relation, removing the mass-dependencies by comparing instead $L_{\rm H\alpha}/L_{\rm bol}$ and $L_{\rm X}/L_{\rm bol}$ does not provide clear evidence for a linear relation. This indicates that chromospheric and coronal activity indicators may be interchangeable in

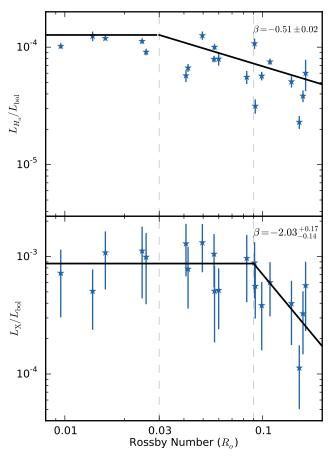


Fig. 10.— $L_{{\rm H}\alpha}/L_{{\rm bol}}$ v. R_o (top) and $L_{{\rm X}}/L_{{\rm bol}}$ v. R_o (bottom) for a sample of M37 stars with both $L_{{\rm H}\alpha}$ and $L_{{\rm X}}$ measurements. Solid lines are the MCMC best-fit parameters (top, for Equation 2; bottom, for equation 2 of Paper I). Vertical lines mark the two threshold $R_{o,{\rm sat}}$ values. The power slopes β are noted in each panel.

—. 2008b, ApJ, 675, 1254 —. 2009, ApJ, 691, 342 activity studies, but only in their pure luminosity forms. We find that $R_{o,\text{sat}}$ is smaller for our chromospheric indicator than for our coronal indicator of activity $(R_{o,\text{sat}} = 0.03\pm0.01 \text{ versus } 0.09\pm0.01)$. We interpret this as possible evidence for coronal stripping, likely a result of both centrifugal forces and an imbalance between mag-

netic and plasma pressure equilibrium.

We thank the SAO Pre-doctoral Program for hosting A.N. for three months at the Harvard Smithsonian Center for Astrophysics in Cambridge, MA. We thank the anonymous referee for comments that improved the paper. M.A.A. acknowledges support provided by the NSF through grant AST-1255419. Support for this work was provided by the National Aeronautics and Space Administration through Chandra Award Number GO6-17039X issued by the Chandra X-ray Observatory Center, which is operated by the Smithsonian Astrophysical Observatory for and on behalf of the National Aeronautics Space Administration under contract NAS8-03060.

This paper makes use of data obtained as part of the INT Photometric H α Survey of the Northern Galactic Plane (IPHAS, www.iphas.org) carried out at the Isaac Newton Telescope (INT). The INT is operated on the island of La Palma by the Isaac Newton Group in the Spanish Observatorio del Roque de los Muchachos of the Instituto de Astrofisica de Canarias. All IPHAS data are processed by the Cambridge Astronomical Survey Unit, at the Institute of Astronomy in Cambridge. The bandmerged DR2 catalogue was assembled at the Centre for Astrophysics Research, University of Hertfordshire, supported by STFC grant ST/J001333/1.

REFERENCES Adelman-McCarthy, J. K. et al. 2007, ApJS, 172, 634 Hodgkin, S. T., Jameson, R. F., & Steele, I. A. 1995, MNRAS, Agüeros, M. A. et al. 2009, ApJS, 181, 444 274. 869 Anglada-Escudé, G. et al. 2016, Nature, 536, 437 Husser, T.-O., Wende-von Berg, S., Dreizler, S., Homeier, D., Argiroffi, C., Caramazza, M., Micela, G., Sciortino, S., Moraux, Reiners, A., Barman, T., & Hauschildt, P. H. 2013, A&A, 553, E., Bouvier, J., & Flaccomio, E. 2016, A&A, 589, A113 Campbell, B., Mein, N., Mein, P., Dumont, S., Cayrel, R., & Irwin, J., Berta, Z. K., Burke, C. J., Charbonneau, D., Nutzman, P., West, A. A., & Falco, E. E. 2011, ApJ, 727, 56 Cayrel de Strobel, G. 1983, A&A, 123, 89 Christian, D. J., Mathioudakis, M., Arias, T., Jardine, M., & Isobe, T., Feigelson, E. D., Akritas, M. G., & Babu, G. J. 1990, Jess, D. B. 2011, ApJ, 738, 164 ApJ, 364, 104 Cram, L. E., & Mullan, D. J. 1985, ApJ, 294, 626 Jackson, R. J., & Jeffries, R. D. 2010, MNRAS, 407, 465 Davenport, J. R. A. 2016, ApJ, 829, 23 Jardine, M., & Unruh, Y. C. 1999, A&A, 346, 883 Douglas, S. T. et al. 2014, ApJ, 795, 161 Jester, S. et al. 2005, AJ, 130, 873 Douglas, S. T., Agüeros, M. A., Covey, K. R., Cargile, P. A., Barclay, T., Cody, A., Howell, S. B., & Kopytova, T. 2016, Kaler, J. B. 1983, ApJ, 271, 188 Kiraga, M., & Stępień, K. 2007, Acta Astronomica, 57, 149 ApJ, 822, 47 Kraus, A. L., & Hillenbrand, L. A. 2007, AJ, 134, 2340 Draine, B. T. 2011, Physics of the Interstellar and Intergalactic Martínez-Arnáiz, R., López-Santiago, J., Crespo-Chacón, I., & Montes, D. 2011, MNRAS, 417, 3100 Medium Drew, J. E. et al. 2005, MNRAS, 362, 753 Messina, S., Distefano, E., Parihar, P., Kang, Y. B., Kim, S.-L., Fabricant, D. et al. 2005, PASP, 117, 1411 Rey, S.-C., & Lee, C.-U. 2008, A&A, 483, 253 Foreman-Mackey, D., Hogg, D. W., Lang, D., & Goodman, J. Noyes, R. W., Weiss, N. O., & Vaughan, A. H. 1984, ApJ, 287, 2013, PASP, 125, 306 769 Frew, D. J., & Parker, Q. A. 2010, PASA, 27, 129 Núñez, A., & Agüeros, M. A. 2016, ApJ, 830, 44 Ginsburg, A., & Mirocha, J. 2011, PySpecKit: Python Núñez, A. et al. 2015, ApJ, 809, 161 Pace, G., & Pasquini, L. 2004, A&A, 426, 1021 Spectroscopic Toolkit, Astrophysics Source Code Library Girardi, L., Grebel, E. K., Odenkirchen, M., & Chiosi, C. 2004, Pallavicini, R., et al. 1981, ApJ, 248, 279 A&A, 422, 205 Parker, E. N. 1960, ApJ, 132, 821 Güdel, M., Guinan, E. F., & Skinner, S. L. 1997, ApJ, 483, 947 -. 1993, ApJ, 408, 707 Hartman, J. D. et al. 2008a, ApJ, 675, 1233 Preibisch, T., & Feigelson, E. D. 2005, ApJS, 160, 390

Randich, S. 2000, in Astronomical Society of the Pacific Conference Series, Vol. 198, Stellar Clusters and Associations: Convection, Rotation, and Dynamos, ed. R. Pallavicini, G. Micela, & S. Sciortino, 401
Rauscher, E., & Marcy, G. W. 2006, PASP, 118, 617
Scandariato, G. et al. 2016, ArXiv e-prints
Schlafly, E. F., & Finkbeiner, D. P. 2011, ApJ, 737, 103
Schwarzenberg-Czerny, A. 1996, ApJ, 460, L107
Skrutskie, M. F. et al. 2006, AJ, 131, 1163

Skumanich, A. 1972, ApJ, 171, 565
Stauffer, J. R., Schultz, G., & Kirkpatrick, J. D. 1998, ApJ, 499, L199 Stelzer, B. et al. 2012, A&A, 537, A94
Stelzer, B., Marino, A., Micela, G., López-Santiago, J., & Liefke, C. 2013, MNRAS, 431, 2063
Strassmeier, K. G., Fekel, F. C., Bopp, B. W., Dempsey, R. C., & Henry, G. W. 1990, ApJS, 72, 191
Strömgren, B. 1939, ApJ, 89, 526
Vaiana, G. S. et al. 1981, ApJ, 245, 163
White, M. L. 1952, ApJ, 115, 71
Wright, N. J., Drake, J. J., Mamajek, E. E., & Henry, G. W. 2011, ApJ, 743, 48
York, D. G. et al. 2000, AJ, 120, 1579